J Comput Neurosci (2007) 23:301–311
DOI 10.1007/s10827-007-0033-y

Threshold fatigue and information transfer

Maurice J. Chacron · Benjamin Lindner · André Longtin

Received: 28 November 2006 / Revised: 8 March 2007 / Accepted: 13 March 2007 / Published online: 14 April 2007

Abstract Neurons *in vivo* must process sensory information in the presence of significant noise. It is thus plausible to assume that neural systems have developed mechanisms to reduce this noise. Theoretical studies have shown that threshold fatigue (i.e. cumulative increases in the threshold during repetitive firing) could lead to noise reduction at certain frequencies bands and thus improved signal transmission as well as noise increases and decreased signal transmission at other frequencies: a phenomenon called noise shaping. There is, however, no experimental evidence that threshold fatigue actually occurs and, if so, that it will actually lead to noise shaping. We analyzed action potential threshold variability in intracellular recordings *in vivo* from pyramidal neurons in weakly electric fish and found experimental evidence for threshold fatigue: an increase in instantaneous firing rate was on average accompanied by an increase in action potential threshold. We show that, with a minor modification, the standard Hodgkin–Huxley model can reproduce this phenomenon. We next compared the performance of models with and without threshold fatigue. Our results show that threshold fatigue will lead to a more regular spike train as well as robustness to intrinsic noise via noise shaping. We finally show that the increased/reduced noise levels due to threshold fatigue correspond to decreased/increased information transmission at different frequencies.

Keywords Action potential threshold · Variability · Information theory · Refractoriness

Action Editor: David Golomb

M. J. Chacron (✉)
Departments of Physiology and Physics, Center for Nonlinear Dynamics, McGill University,
Montreal H3G-1Y6, Canada
e-mail: maurice.chacron@mcgill.ca

B. Lindner · A. Longtin
Department of Physics, University of Ottawa,
Ottawa K1N-6N5, Canada

B. Lindner
Max Planck Institute for the Physics of Complex Systems,
Nöthnitzer Str. 38,
01187 Dresden, Germany

1 Introduction

Neurons must transmit information about incoming stimuli reliably and efficiently in order for animals to survive in their environment (Rieke et al. 1996). However, most neurons display considerable variability even to repeated presentations of the same stimulus (Bryant and Segundo 1976; Softky and Koch 1993; Mainen and Sejnowski 1995). Whether this variability is to be considered as noise or part of the signal is still being debated (Stein et al. 2005). However, it is almost certain that at least part of the variability displayed by neurons *in vivo* is due to intrinsic (e.g. flicker noise) or extrinsic noise sources (noise in the environment or from synaptic bombardment) (Manwani and Koch 1999). There is thus great interest in understanding the mechanisms by which neurons encode sensory stimuli in the presence of noise.

Many electronic devices such as Sigma-Delta modulators and Josephson junctions must also operate in the presence of noise (Wiesenfeld and Satija 1987; Norsworthy et al. 1997; Yacomotti et al. 1999). This operation is facilitated through a phenomenon called noise shaping: noise power is shifted from one frequency range to another thereby improving signal transmission in the former frequency range and worsening it in the latter. It has been proposed that the brain might use noise shaping (Shin 1993,

2001) and modeling studies have shown that this phenomenon could occur both at the network (Mar et al. 1999) and at the single neuron level (Chacron et al. 2004a; Lindner et al. 2005). In the latter case, it was shown theoretically and through numerical simulations that spike trains with negative interspike interval (ISI) correlations displayed lower variability at low frequencies (i.e, noise shaping), thereby improving information transmission of sensory stimuli containing these frequencies (Chacron et al. 2004a; Lindner et al. 2005). Further experimental work then showed that the electroreceptor afferents of electric fish displayed noise shaping (Chacron et al. 2005b).

Theoretical and modeling studies have shown that several mechanisms could give rise to negative ISI correlations. These include threshold fatigue: a cumulative increase in the action potential threshold following rapid firing (Geisler and Goldberg 1966; Holden 1976; Chacron et al. 2001b; Liu and Wang 2001; Chacron et al. 2003a; Jolivet et al. 2006). There is however, to our knowledge, no experimental evidence that an actual increase in action potential threshold occurs during repetitive firing although several modeling studies have made detailed predictions on the effects of threshold fatigue on adaptation depending on various parameters (Geisler and Goldberg 1966; Holden 1976; Koch 1999; Liu and Wang 2001; Chacron et al. 2003a), and information transmission (Chacron et al. 2001b). Furthermore, the simplified models used in previous studies were phenomenological in nature and it is not clear how to include threshold fatigue, should it exist, in more realistic biophysical neuron models such as the one proposed by Hodgkin and Huxley (1952) where the action potential threshold can only be defined phenomenologically.

In this paper, we demonstrate that pyramidal neurons within the electrosensory lateral line lobe of weakly electric fish display threshold fatigue *in vivo*: the action potential threshold is shown to increase following periods of rapid action potential firing and is shown to decrease during periods of silence. This results in a covariation between the instantaneous firing rate and the action potential threshold which can be detected in experimental recordings. Our results furthermore show that threshold fatigue is most present in neurons with high firing rates. Thus, threshold fatigue is most likely due to refractory effects in sodium channels such as desensitization (Mickus et al. 1999). Although the standard Hodgkin–Huxley model cannot reproduce this phenomenon, we propose an extended Hodgkin–Huxley model that reproduces the threshold fatigue seen experimentally. Finally, we investigated the effects of threshold fatigue in our model. We show that threshold fatigue not only leads to noise shaping as predicted from theoretical studies, but also leads to a more regular spike train as well as sensitivity to a larger range of stimulus intensities as well as increased information transmission.

2 Materials and methods

2.1 Experimental recordings

We used the weakly electric fish *Apteronotus leptorhynchus* in this study and the experimental protocol has been described in detail previously (Bastian et al. 2002; Chacron 2006). Briefly, animals were immobilized by intramuscular injection of curare and respirated with aerated water at a flow of 10 ml/min. Intracellular recordings from pyramidal cells in the electrosensory lateral line lobe were made with glass micropipettes (resistance 25–40 MΩ) filled with 3 M KCL. Recording sites as determined from surface landmarks and depth were limited to the centrolateral and lateral segments only. Sensory stimulation was achieved by presenting amplitude modulations (AMs) of the animal's own quasi-sinusoidal electric organ discharge via two electrodes located 20 cm on each side of the animal. The AM consisted of low-pass filtered Gaussian white noise (120 Hz cutoff, 8th order Butterworth filter). All procedures were approved by McGill University's animal care committee.

2.2 Modified Hodgkin–Huxley model

We used a Hodgkin–Huxley model with leak, sodium, and potassium conductances. The model is described by the following equations:

$$C\frac{dV}{dt} = -g_{leak}(V - E_{leak}) - g_{na}\, m^3 h(V - E_{na}) - g_k n^2 (V - E_k) + \xi(t) + I + S(t)$$

$$\frac{dm}{dt} = \frac{m_\infty(V) - m}{\tau_m}$$

$$\frac{dh}{dt} = \frac{h_\infty(V) - h}{\tau_h}$$

$$\frac{dn}{dt} = \frac{n_\infty(V) - n}{\tau_n}$$

Here V is the membrane potential expressed in mV, g_x is the maximum conductance of channel x and E_x is its reversal potential, $\xi(t)$ is Gaussian white noise with zero mean and autocorrelation function $<\xi(t)\ \xi(t+\tau)>=\sigma^2\ \delta(\tau)$, I is the

applied current, and $S(t)$ is the stimulus which consists of low-passed filtered Gaussian white noise with spectral height α and cutoff frequency f_c. The infinite conductance curves are given by:

$$m_\infty(V) = \frac{1}{1+\exp\left[-(V-V_{1/2})/3\right]}$$
$$h_\infty(V) = \frac{1}{1+\exp\left[(V-V_{1/2})/3\right]}$$
$$n_\infty(V) = \frac{1}{1+\exp\left[-(V-40)/3\right]}$$

Usually, $V_{1/2}$ is taken to be constant (Hodgkin and Huxley 1952). We instead make $V_{1/2}$ vary with time:

$$\frac{dV_{1/2}}{dt} = -\frac{55+V_{1/2}}{\tau_V} + 12\sum_{i=1}^{\infty}\delta(t-t_i)$$

where t_i is the timing of the ith action potential. This implies that $V_{1/2}$ is increased by 12 mV immediately after each action potential and is then allowed to relax back to its equilibrium value of −55 mV. The differential equation for $V_{1/2}$ is exactly the same as that governing the time varying threshold in more phenomenological models (Geisler and Goldberg 1966; Chacron et al. 2001b; Liu and Wang 2001). This is motivated by the fact that $V_{1/2}$ is closely related to the action potential threshold as measured in this study since it is the voltage at which roughly 50% of sodium channels are open.

We used an Euler–Maruyama integration scheme for numerical simulations with time step dt=25 μs. Parameter values used were: g_{na}=55 μS, g_k=40 μS, g_{leak}=0.18 μS, E_{leak}=−70 mV, E_{na}=40 mV, E_k=−88.5 mV, τ_m=0.02 ms, τ_h=τ_n=0.39 ms, τ_V=40 ms, σ=I=1 nA. The model gave rise to sustained action potential firing in the absence of noise (i.e. σ=0).

2.3 Data analysis

We computed the threshold value for spike time t_{i+1}, θ_i, as the membrane potential value at the time at which the second derivative of the membrane potential was maximum (see Fig. 1). We note that, while this procedure is different than the one previously proposed (Azouz and Gray 1999, 2000), our results do not qualitatively depend on which of the two algorithms is used to compute the action potential threshold (data not shown).

The interspike interval sequence (ISI), the sequence of times between consecutive action potentials, $\{I_i\} \equiv \{t_{i+1} - t_i\}$ was obtained from the spike time sequence $\{t_i\}$. We computed the ISI serial correlation coefficients ρ_j as:

$$\rho_j = \frac{< I_i I_{i+j} > - < I_i >^2}{< I_i^2 > - < I_i >^2}$$

Where the average <…> is taken over index i. From the ISI sequence, we obtained the instantaneous firing rate sequence as $\{f_i\} \equiv \{1/I_i\}$ and the cross-correlation coefficient between $\{\theta_i\}$ and $\{f_i\}$ was then computed as:

$$C_j = \frac{< f_i \theta_{i+j} > - < f_i >< \theta_i >}{\sqrt{< f_i^2 > - < f_i >^2}\sqrt{< \theta_i^2 > - < \theta_i >^2}}$$

For signal transmission analysis, the stimulus $S(t)$ was sampled at 2 kHz and we made a binary representation R of the spike train at 2 kHz also. We then computed the stimulus-spike train coherence as (Rieke et al. 1996):

$$C_{RS}(f) = \frac{|P_{RS}(f)|^2}{P_{RR}(f)P_{SS}(f)}$$

where $P_{RS}(f)$ is the cross-spectrum between the stimulus and the binary sequence and $P_{RR}(f)$, $P_{SS}(f)$ are the power spectra of the binary sequence and stimulus, respectively. The coherence ranges between 0 and 1 and measures the correlation between the stimulus and neural response at frequency f. The coherence is furthermore related to the mutual information density between the stimulus and response by: $I = -\log_2[1 - C_{RS}(f)]$ (Rieke et al. 1996). We normalized the mutual information density I by the firing rate to account for its known dependence on firing rate (Borst and Haag 2001).

We used a threshold interspike interval value of 20 ms for classifying spikes as either being part of a burst or not

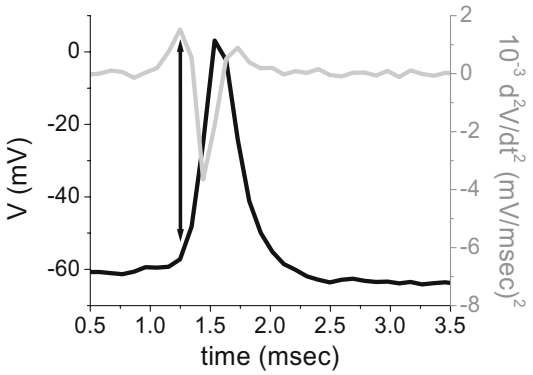

Fig. 1 Illustration of the procedure to compute the action potential threshold. We computed the second derivative (*gray*) of the membrane potential (*black*) and computed the time at which the second derivative was maximal (*arrow*). The threshold value was calculated as the value of the membrane potential at that time

(Gabbiani et al. 1996; Metzner et al. 1998; Chacron et al. 2004c; Oswald et al. 2004). As such, an ISI was considered to be part of a burst only if it was smaller than the threshold and we constructed from the binary sequence R a binary sequence R_{bursts} with all the spikes that belonged to bursts.

3 Results

3.1 Sensory neurons display threshold fatigue

Figure 1 illustrates the method to compute the action potential threshold. We took the action potential threshold as the point of greatest curvature of the membrane potential V as determined by the local maximum of the second derivative. We then applied this algorithm to intracellular recordings from pyramidal cells in the electrosensory lateral line lobe of weakly electric fish. An example cell is shown in Fig. 2. Visual inspection of the membrane potential (Fig. 2(a)) shows that the action potential threshold is variable and ranges between −62 and −57 mV for this particular cell (Fig. 2(b)). A more careful visual inspection shows that the action potential threshold actually increases during periods of rapid firing and decreases during periods of silence (Fig. 2(a)). This is most easily seen by comparing the time evolution of the threshold to that of the instantaneous firing rate (Fig. 2(c)). It is seen that periods of elevated firing are associated with higher threshold, leading to a positive correlation coefficient (Fig. 2(d)) as well as negative correlation coefficient in adjacent lags. This neuron also showed a prominent negative ISI correlation coefficient at lag one (ρ_1=−0.2988) (Fig. 2(d), inset).

3.2 Threshold fatigue is most prominent in neurons with high spontaneous firing rates

Previous studies have shown that the pyramidal cell population was heterogeneous both anatomically and physiologically. There is a strong negative correlation between spontaneous firing rate and dendritic morphology: cells with small dendritic trees tend to have large firing rates while cells with large dendritic trees tend to have small firing rates (Bastian and Nguyenkim 2001; Bastian et al. 2004). Figure 3(a) assesses the influence of firing rate on threshold fatigue as quantified by the cross-correlation coefficient between threshold and reciprocal interspike interval (ISI) at lag 0 C_0. A strong positive correlation (R=0.64, p=0.00163, N=21) was observed, meaning that threshold fatigue is more likely to be observed in neurons with large firing rates. Previous modeling studies have shown that threshold fatigue can be associated with negative ISI correlations at lag 1 (i.e. short interspike intervals are on average followed by long ones and vice-versa) (Chacron et al. 2000, 2001b, 2003a; Liu and Wang 2001). We thus plotted the ISI correlation coefficient at lag 1 ρ_1 as function of firing rate (Fig. 3(b)). A strong negative correlation between ρ_1 and firing rate was observed (R=−0.823, p<0.0001, N=21), indicating that cells with high spontaneous firing rates also tended to display negative ISI correlations. Thus, as predicted from theory (Chacron et al.

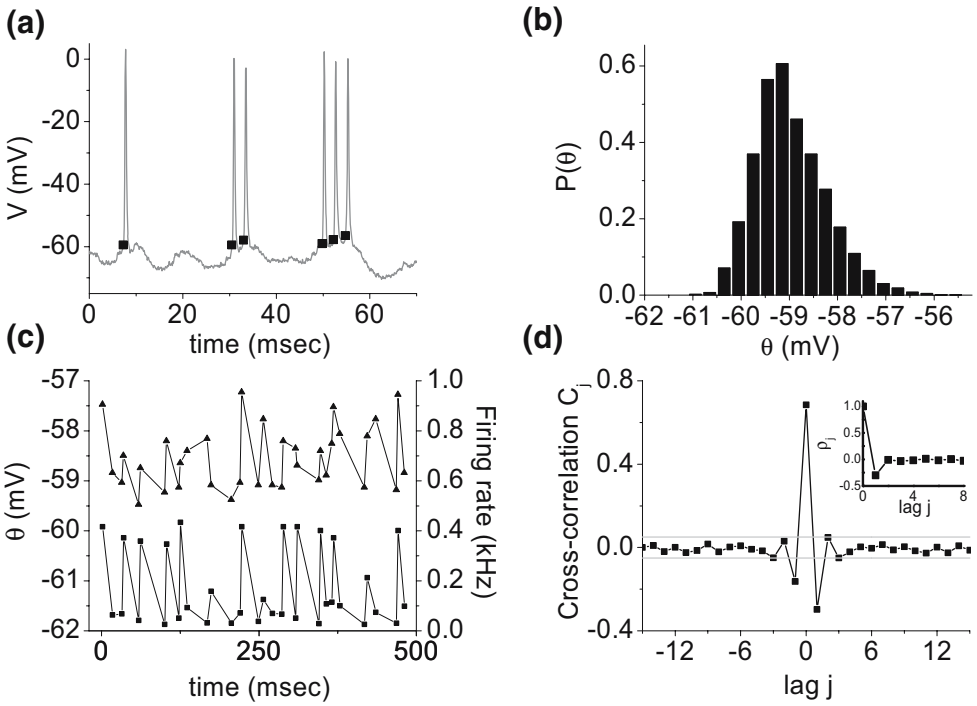

Fig. 2 Sensory neurons show threshold fatigue *in vivo*. (**a**) Membrane potential (*gray*) and action potential threshold (squares). (**b**) Probability density for the threshold θ. (**c**) Action potential threshold (*squares*) and instantaneous firing rate (*triangles*). (**d**) Cross-correlation function between the threshold and instantaneous firing rate. The *gray lines* show the 99% confidence interval. The *inset* shows the cross-correlation coefficients ρ_j as a function of lag j. Only ρ_0 and ρ_1 are significantly different from 0

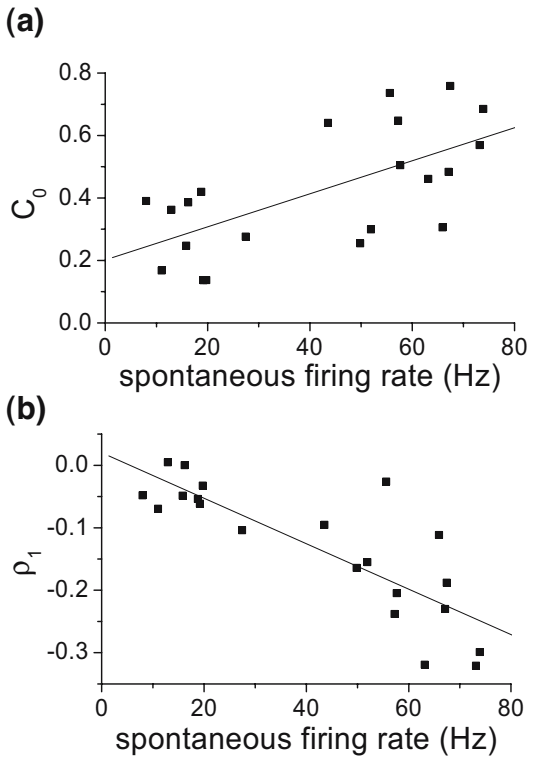

Fig. 3 Effects of pyramidal cell heterogeneities seen *in vivo* on threshold fatigue. (**a**) Cross-correlation coefficient at lag 0 (C_0) as a function of spontaneous firing rate. (**b**) ISI correlation coefficient at lag 1 (ρ_1) as a function of spontaneous firing rate

2004a; Lindner et al. 2005), cells that displayed threshold fatigue also tended to display a negative ISI correlation coefficient at lag 1.

3.3 A biophysical model of threshold fatigue

Although many phenomenological models have proposed variations in the action potential threshold (Geisler and Goldberg 1966; Gestri et al. 1980; Gabbiani and Koch 1996; Chacron et al. 2001b, 2004a), it was only recently shown that more biophysically realistic models such as the Hodgkin–Huxley model displayed threshold variability (Azouz and Gray 1999). We thus tested whether a realistic biophysical model with Hodgkin–Huxley conductances, which has been shown to display threshold variability (Azouz and Gray 1999), could display threshold fatigue. The results are shown in Fig. 4. Although the model does display variability in the action potential threshold (Fig. 4(a,b)), there are no cumulative increases in threshold during rapid firing and there is no significant correlation between the instantaneous firing rate and the threshold (Fig. 4(c,d)). The model furthermore displayed no significant ISI correlations at lag 1 (ρ_1=−0.00152) (Fig. 4(d), inset).

Previous studies have shown that pyramidal cells had a well characterized burst mechanism that relies on an interaction between somatic and dendritic voltage-gated sodium channels (Lemon and Turner 2000; Doiron et al.

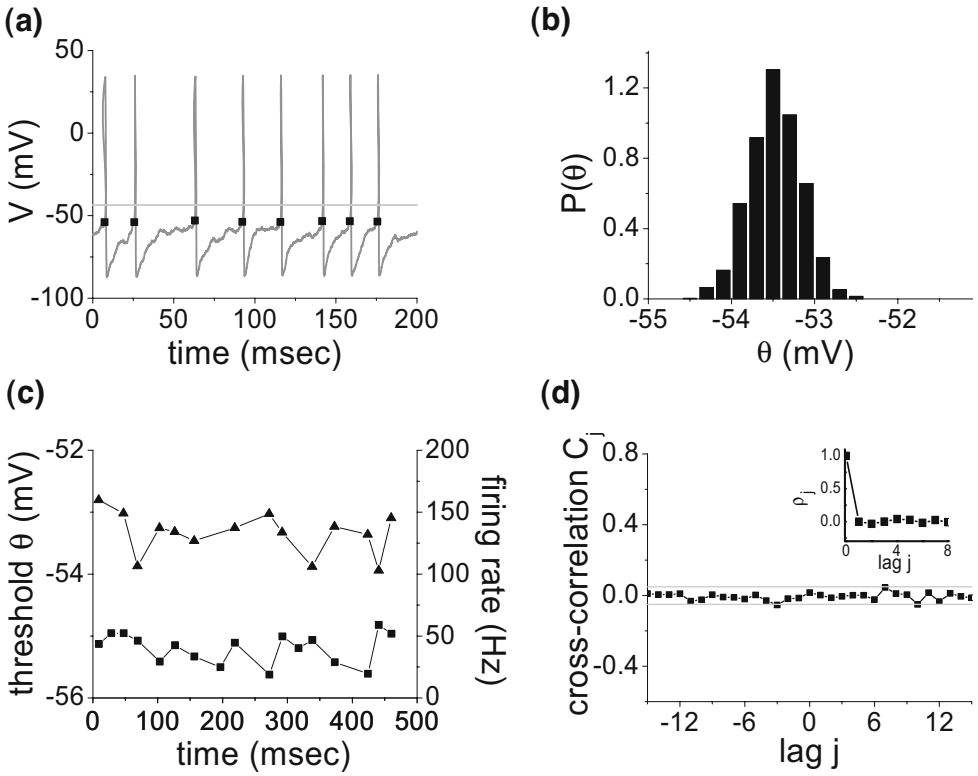

Fig. 4 The Hodgkin–Huxley model with constant $V_{1/2}$ does not display threshold fatigue. (**a**) Voltage (*gray*) and threshold (*black squares*) from the model. The *light gray horizontal line* shows the constant value $V_{1/2}$=−43.581 mV used in the simulations. (**b**) Probability density for the threshold θ. (**c**) Action potential threshold (*squares*) and instantaneous firing rate (*triangles*). (**d**) Cross-correlation function between the threshold and instantaneous firing rate. The *gray lines* indicate the 99% confidence interval. The *inset* shows ρ_j as a function of *j*. Only ρ_0 is significantly different from 0. The inset Parameter values used for the stimulus were: α=0.0167 nA^2/Hz, f_c=120 Hz. The mean firing rate was 32.43 Hz

2002; Fernandez et al. 2005). Although burst dynamics can sometimes give rise to negative ISI correlations (Chacron et al. 2001a), this particular mechanism does not seem to be sufficient to generate the negative ISI correlations and threshold fatigue seen in our experimental data as revealed by simulations of the model proposed by Doiron et al. (2002) (data not shown).

Thus, we explored additions to the Hodgkin–Huxley model that could reproduce the experimental data. We varied the inflexion point of the activation and inactivation infinite conductance curves of the sodium conductance, $V_{1/2}$, in a dynamic manner similar to the threshold in phenomenological models (Chacron et al. 2001b, 2003a; Liu and Wang 2001). The results are shown in Fig. 5. With this minor modification, the model exhibits threshold fatigue: the threshold increases during repetitive firing (Fig. 5(a)) and displays threshold variability that is similar to the experimental data (Fig. 5(b)). There was a strong positive correlation between the instantaneous firing rate and the threshold (Fig. 5(c,d)) as in the experimental data. The model furthermore displayed a significant ISI correlation coefficient at lag 1 (ρ_1=−0.3349) that was similar in magnitude to that seen experimentally (Fig. 5(d), inset). We note that the model does not reproduce the damped oscillation in the cross-correlation observed for the data, such a damped oscillation might be due to underlying network dynamics (Doiron et al. 2003). However, a simple point-process model (i.e. no spatial structure) is sufficient to qualitatively explain the threshold fatigue and negative ISI correlations seen in pyramidal cells.

3.4 Effects of firing rate on threshold fatigue in the model

In order to vary the firing rate in the model with threshold fatigue, we varied the bias current I. Figure 6 shows the effects of varying the bias current on the ISI correlation coefficient at lag 1, and the cross-correlation coefficient between the instantaneous firing rate and the action potential threshold. Both the ISI correlation coefficient (Fig. 6(a)) and the cross-correlation coefficient (Fig. 6(b)) increased in magnitude as a function of firing rate thereby reproducing experimental results (Fig. 3). As such, our model qualitatively explains the variations seen in experimental data and predicts that these are predominantly due to differences in firing rate amongst pyramidal cells. The effects seen can be explained as follows: reducing the bias current reduces the firing rate, thereby increasing the mean ISI. There is therefore less accumulation in threshold during rapid firing, which leads to a decrease in the ISI correlation coefficient (ρ_1) and the cross-correlation coefficient (C_0). The decrease in ρ_1 as a function of firing rate is similar to previous results obtained with phenomenological models (Liu and Wang 2001; Chacron et al. 2003a).

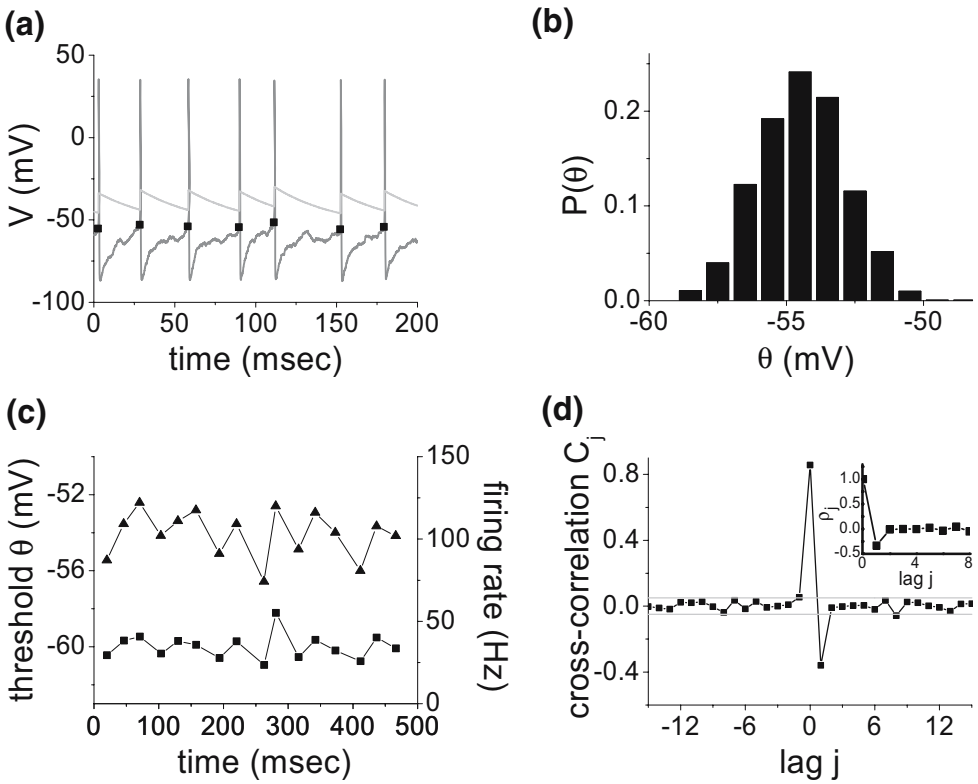

Fig. 5 The Hodgkin–Huxley model with dynamic $V_{1/2}$ exhibits threshold fatigue. (**a**) Voltage (*gray*) and threshold (*black squares*) from the model. The *light gray* trace shows the time evolution of $V_{1/2}$=−43.581. (**b**) Probability density for the threshold θ. (**c**) Action potential threshold (*squares*) and instantaneous firing rate (*triangles*). (**d**) Cross-correlation function between the threshold and instantaneous firing rate. The *gray lines* indicate the 99% confidence interval. The *inset* shows ρ_j as a function of j. As in the experimental data, both ρ_0 and ρ_1 are significantly different from 0. Parameter values used for the stimulus were: α= 0.0167 nA^2/Hz, f_c=120 Hz. The mean firing rate was 31.64 Hz

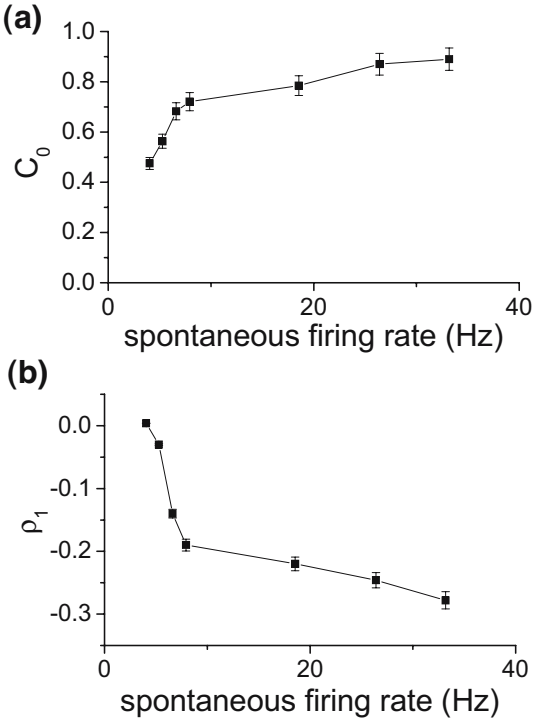

Fig. 6 Effects of varying the bias current I on the firing rate, the cross-correlation coefficient at lag 0 (C_0) and the ISI correlation coefficient (ρ_1) in the model. (**a**) Cross-correlation coefficient at lag 0 (C_0) as a function of spontaneous firing rate. (**b**) ISI correlation coefficient at lag 1 (ρ_1) as a function of spontaneous firing rate. Parameter values used were the same as for Fig. 5. The values of I used were, in increasing order of firing rates, −2,−1.8,−1.6,−1.4,0,1,2. The *error bars* show the standard error on the quantities based on ten simulations

3.5 Threshold fatigue regularizes firing and confers robustness to noise

We quantified the effects of threshold fatigue by comparing the performance of the model with dynamic $V_{1/2}$ to that of the model with constant $V_{1/2}$, henceforth referred to as the model without threshold fatigue. Overall, the model with threshold fatigue produced spike trains that were more regular than those produced by the model without threshold fatigue as seen by looking at the ISI distribution (Fig. 7(a)). The coefficient of variation (CV, standard deviation to mean ratio of the ISI distribution) was 0.21 with threshold fatigue and 0.44 without. The power spectra of spike trains (Fig. 7(b)) also indicate less output noise in the case of threshold fatigue: power at low frequencies is reduced and the peak at the neuron's firing rate (about 30 Hz) becomes much sharper. These effects are a consequence of diminished ISI variability (lower CV) and negative correlations among ISIs $\sum_{i=1}^{\infty}\rho_j < 0$ both caused by threshold fatigue. In particular, in the low frequency limit it is known that $S(f=0) = \mathrm{CV}^2 r\left[1+2\sum_{i=1}^{\infty}\rho_j\right]$ for a stationary spike train (Cox and Lewis 1966; Holden 1976), hence both a decrease in CV and the presence of negative correlations lead to a drop in low-frequency power. We note that these results are similar to previous ones using more phenomenological models (Chacron et al. 2004a,b; Lindner et al. 2005) as well as experimental results (Chacron et al. 2005b).

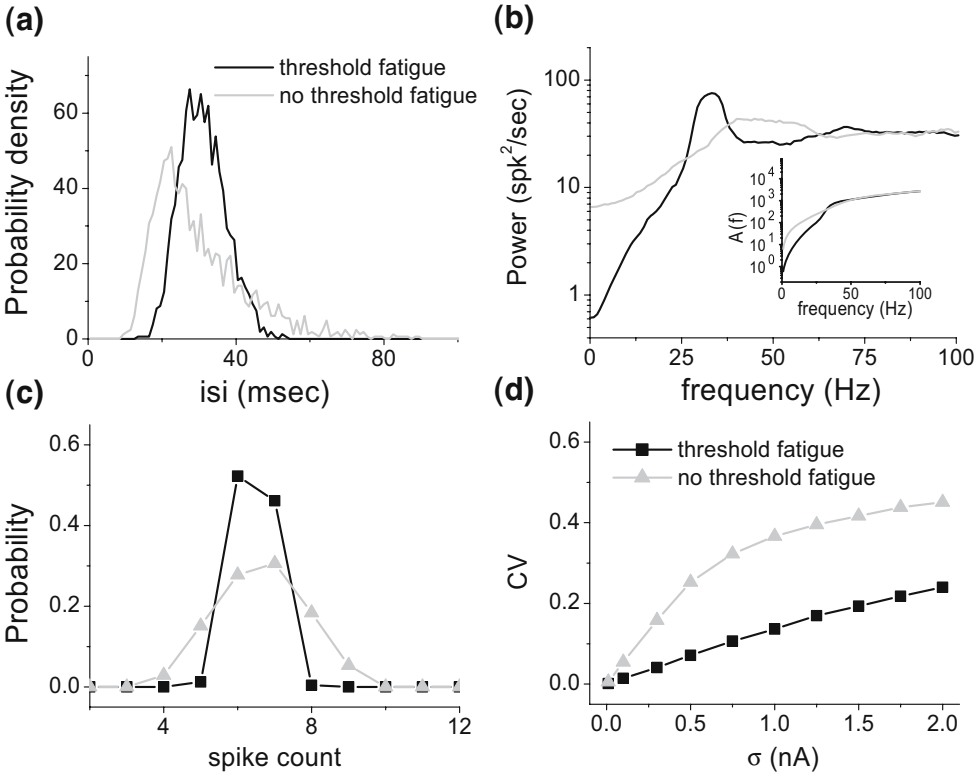

Fig. 7 Threshold Fatigue regularizes the spike train in the absence of stimulation. (**a**) ISI distributions obtained with (*black*) and without (*gray*) threshold fatigue. (**b**) Spike train power spectrum with (*black*) and without (*gray*) threshold fatigue. The *inset* shows the area under each spectrum up to frequency f as a function of f. (**c**) Spike count distributions obtained for a 200 ms time window with (*black squares*) and without (*gray triangles*) threshold fatigue. (**d**) Coefficient of variation (CV) versus noise standard deviation σ. Parameters values were the same as in Fig. 5 except α=0 for panel (**d**)

We also computed the area $A(f)$ between 0 and frequency f under each power spectrum. The areas computed with and without threshold fatigue are equal for $f > 60$ Hz, confirming that this is indeed a reshaping of the power spectrum (Fig. 7(b), inset) (i.e. the total power is conserved). The spike count distribution (Barlow and Levick 1969a,b; Teich and Khanna 1985) also displayed less variance with threshold fatigue (Fig. 7(c)). We also varied the noise standard deviation σ and found that spike train variability, as quantified by CV, was generally lower in the presence of threshold fatigue (Fig. 7(d)). As such, the model with threshold fatigue is more robust to noise than the model without threshold fatigue.

3.6 Threshold fatigue and information transmission

We finally quantified the effects of threshold fatigue on information transmission. However, the models with and without threshold fatigue gave rise to very different ISI probability densities (Fig. 7(a)). In particular, the probability density of high frequency ISIs (<20 ms) was lower for the model with threshold fatigue than for the model without threshold fatigue. Since previous studies have shown that high frequency ISIs coded for low frequency stimuli (Oswald et al. 2004), we compared information transmission by high frequency ISIs with and without threshold fatigue. The results are shown in Fig. 8 were the information densities normalized by the event rates are compared. It is seen that, for low (<20 Hz) and higher frequencies (38–60 Hz), the model with threshold fatigue had a larger information density than the model without threshold fatigue. The situation was opposite however in the intermediate frequency range (20–38 Hz). A stimulus with power only in this range would thus be best transmitted with a neuron without threshold fatigue as predicted from theory (Lindner et al. 2005). This confirms that the noise shaping seen in the power spectrum does translate to increased information transmission. Though threshold fatigue will give rise to less high frequency ISIs, each one will transmit a greater amount of information as there is less noise.

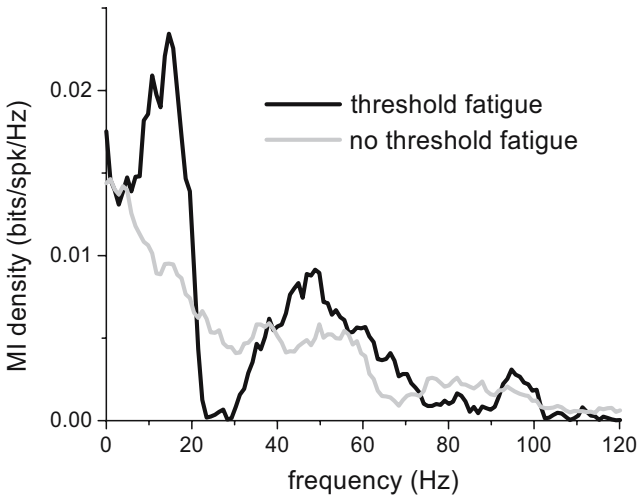

Fig. 8 Noise shaping and information transmission. Shown are the mutual information densities for the burst spike train (20 ms burst threshold) obtained with the model with (*black*) and without (*gray*) threshold fatigue. Parameter values were the same as in Fig. 5(c)

4 Discussion

We have shown that sensory neurons *in vivo* displayed variations in the action potential threshold in the form of threshold fatigue and that this phenomenon was accompanied by action potential patterning in the form of negative interspike interval correlations. There was a strong dependence on the mean firing rate of the neuron in that neurons with high firing rates were most likely to display threshold fatigue. It was furthermore shown that a standard Hodgkin–Huxley model, although capable of displaying action potential threshold variability, could not reproduce threshold fatigue. We showed that cumulative refractoriness through changes in the activation and inactivation voltages of sodium channels was necessary to reproduce the experimental data. Changes in threshold fatigue for different firing rates similar to those seen in the experimental data could be obtained by varying the bias current in the model with threshold fatigue. Finally, we showed that addition of threshold fatigue lead to noise shaping as well as increased information transmission, which confirms previous theoretical studies.

Recent theoretical and modeling studies have shown that negative interspike interval correlations would lead to noise shaping as well as increased information transmission (Chacron et al. 2001b, 2004a; Lindner et al. 2005). However, these correlations can result from very different biophysical mechanisms. One example is the cumulative activation of an outward current (Treves 1996; Liu and Wang 2001) such as a calcium-activated potassium current (Wang 1998). These currents are omnipresent in the central nervous system (Sah 1996). Our results also show that threshold fatigue can give rise to the same effects qualitatively. In fact, it was shown that a phenomenological model incorporating threshold fatigue was qualitatively equivalent to a model incorporating a spike activated outward current (Liu and Wang 2001). Different biophysical mechanisms might thus serve the same function in the central nervous system.

While many neurons show no spontaneous activity, many neurons such as auditory fibers (Köppl 1997),

vestibular afferents (Goldberg 2000), neocortical neurons in awake behaving animals (Steriade 1978), electroreceptor afferents (Bastian 1981), deep cerebellar nuclei neurons (Aizenman and Linden 1999), and purkinje cells (Jaeger and Bauer 1994) display spontaneous activity (i.e. in the absence of stimulation). In many cases (auditory fibers, vestibular afferents, purkinje cells), the spontaneous firing rate can exceed 100 Hz and these neurons are thus likely to display threshold fatigue according to our results. There is in fact evidence that auditory fibers (Teich 1992) and cortical neurons (Lebedev and Nelson 1996) both display negative ISI correlations which are associated with threshold fatigue. It is thus likely that noise shaping is being used in the brain at multiple levels.

We note that previous studies have shown action potential threshold variability in cortical neurons (Azouz and Gray 1999, 2000). However, in these studies, the action potential threshold variability was due to variations in the slope of the membrane voltage as it reached the action potential threshold. Azouz and Gray (1999, 2000) observed a negative correlation between the membrane potential slope and the action potential threshold and showed that a standard Hodgkin–Huxley model with sodium and potassium conductances could reproduce this feature. As periods of high firing rates are typically associated with a higher membrane potential slope, one would expect that the action potential threshold actually be lower during such periods. This is contrary to our observations. However, we note that Azouz and Gray (1999, 2000) were studying cortical neurons with low firing rates that most likely will not display threshold fatigue according to our results.

A decreased action potential threshold during periods of elevated firing would lead to increased coincidence detection (Azouz and Gray 1999, 2000). These effects are most likely to be found in neurons with low firing rates. Such neurons are most likely to act as feature detectors as they will transmit less information about the detailed time course of the stimulus due to their low firing rates (Borst and Haag 2001). However, threshold fatigue is most likely to be found in neurons with high firing rates according to our results. Such neurons will transmit more information about the detailed time course of the stimulus due to their high firing rates (Borst and Haag 2001); furthermore, noise shaping due to threshold fatigue will increase this information as predicted from theoretical and experimental studies (Chacron et al. 2004a, 2005b; Lindner et al. 2005). These neurons might act as temporal integrators to transmit information about the detailed time course of the stimulus. This is consistent with previous results obtained on the pyramidal cells population of weakly electric fish: pyramidal cells with low firing rates respond to specific features of the stimulus (Gabbiani et al. 1996; Metzner et al. 1998; Bastian et al. 2002; Chacron et al. 2005a, Chacron 2006) while pyramidal cells with high firing rates are broadly tuned (Chacron et al. 2005a,b, Chacron 2006). This is furthermore consistent with the fact that threshold fatigue, as it is associated with refractoriness, will typically act to suppress burst firing which is associated with feature detection (Sherman 2001). This might explain why pyramidal cells with high firing rates are much more regular than pyramidal cells with low firing rates as quantified by the coefficient of variation (CV) (Bastian and Nguyenkim 2001).

We note that neurons in general show tremendous variability during both spontaneous activity (Burns and Webb 1970; Rudolph and Destexhe 2003) and during stimulation (Shinomoto et al. 1999; Rudolph and Destexhe 2003). How can this variability as measured by coefficient of variations on the order of 1 be reconciled with threshold fatigue which acts to regularize the spike train? First, we note that pyramidal cells in weakly electric fish also display high CVs that range between 0.7 and 1.75 (Bastian and Nguyenkim 2001). As such, threshold fatigue is not necessarily incompatible with the high CVs obtained experimentally. Neurons *in vivo* receive large amounts of synaptic bombardment which contributes to their variability (Rudolph and Destexhe 2003). However, neurons *in vivo* are also capable of precise spike timing under stimulated conditions (Reinagel and Reid 2000; Chacron et al. 2003b). Our results show that threshold fatigue will regularize the spike train and this could, in principle, reduce the overall amount of information transmitted. However, information is the difference between the entropy of the spike train, H(R), and the entropy of the spike train given the stimulus, H(R/S) (Shannon 1948; Cover and Thomas 1991). The latter term is related to the precision of spike timing under stimulated conditions (Mainen and Sejnowski 1995; Reinagel and Reid 2000). Previous results have shown that addition of threshold fatigue in a model will reduce both terms (Chacron et al. 2001b). However, the reduction in H(R/S) is greater than the reduction in H(R), thus giving rise to increased information (Chacron et al. 2001b, 2004a,b; Lindner et al. 2005). As such, threshold fatigue could explain why neurons displaying large amounts of variability can surprisingly display precise spike timing (Reinagel and Reid 2000; Chacron et al. 2003b).

Finally, most neural populations will display significant heterogeneities in both morphology and physiology (Sadeghi et al. 2007). The function advantages, if any, of having a heterogeneous population are not well understood to this day. Our results suggest that threshold fatigue would confer properties only to a subset of neurons and this might optimize coding of sensory information at the population level.

Acknowledgement We thank J. Benda for useful discussions. This research was supported by CIHR (M.J.C., A.L.) and NSERC (A.L.).

References

Aizenman, C. D., & Linden, D. J. (1999). Regulation of the rebound depolarization and spontaneous firing patterns of deep nuclear neurons in slices of rat cerebellum. *Journal of Neurophysiology*, *82*, 1697–1709.

Azouz, R., & Gray, C. M. (1999). Cellular mechanisms contributing to response variability of cortical neurons *in vivo*. *Journal of Neuroscience*, *19*, 2209–2223.

Azouz, R., & Gray, C. M. (2000). Dynamic Spike Threshold reveals a mechanism for synaptic coincidence detection in cortical neurons *in vivo*. *Proceedings of the National Academy of Sciences of the United States of America*, *97*, 8110–8115.

Barlow, H. B., & Levick, W. R. (1969a). Changes in the maintained discharge with adaptation level in the cat retina. *Journal of Physiology (London)*, *202*, 699–718.

Barlow, H. B., & Levick, W. R. (1969b). Three factors limiting the reliable detection of light by the retinal ganglion cells of the cat. *Journal of Physiology (London)*, *200*, 1–24.

Bastian, J. (1981). Electrolocation I. How the electroreceptors of Apteronotus albifrons code for moving objects and other electrical stimuli. *Journal of Comparative Physiology A*, *144*, 465–479.

Bastian, J., & Nguyenkim, J. (2001). Dendritic Modulation of Burst-like firing in sensory neurons. *Journal of Neurophysiology*, *85*, 10–22.

Bastian, J., Chacron. M. J., & Maler, L. (2002). Receptive field organization determines pyramidal cell stimulus-encoding capability and spatial stimulus selectivity. *Journal of Neuroscience*, *22*, 4577–4590.

Bastian, J., Chacron, M. J., & Maler, L. (2004). Plastic and non-plastic cells perform unique roles in a network capable of adaptive redundancy reduction. *Neuron*, *41*, 767–779.

Borst, A., & Haag, J. (2001). Effects of mean firing on neural information rate. *Journal of Computational Neuroscience*, *10*, 213–221.

Bryant, H. L., & Segundo, J. P. (1976). Spike initiation by transmembrane current: a white-noise analysis. *Journal of Physiology*, *260*, 279–314.

Burns, B. D., & Webb, A. C. (1970). Spread of responses in the cerebral cortex to meaningful stimuli. *Nature*, *225*, 469–470.

Chacron, M. J. (2006). Nonlinear information processing in a model sensory system. *Journal of Neurophysiology*, *95*, 2933–2946.

Chacron, M.J., Longtin, A., St-Hilaire, M., & Maler, L. (2000). Suprathreshold stochastic firing dynamics with memory in P-type electroreceptors. *Physical Review Letters*, *85*, 1576–1579.

Chacron, M. J., Longtin, A., & Maler, L. (2001a). Simple models of bursting and non-bursting electroreceptors. *Neurocomputing*, *38*, 129–139.

Chacron, M. J., Longtin, A., & Maler, L. (2001b). Negative interspike interval correlations increase the neuronal capacity for encoding time-varying stimuli. *Journal of Neuroscience*, *21*, 5328–5343.

Chacron, M. J., Pakdaman, K., & Longtin, A. (2003a). Interspike interval correlations, memory, adaptation, and refractoriness in a leaky integrate-and-fire model with threshold fatigue. *Neural Computation*, *15*, 253–278.

Chacron, M. J., Doiron, B., Maler, L., Longtin, A., & Bastian, J. (2003b). Non-classical receptive field mediates switch in a sensory neuron's frequency tuning. *Nature*, *423*, 77–81.

Chacron, M. J., Lindner, B., & Longtin, A. (2004a). Noise shaping by interval correlations increases information transfer. *Physical Review Letters*, *92*, 080601.1–080601.4.

Chacron, M. J., Lindner, B., & Longtin, A. (2004b). ISI correlations and information transfer. *Fluctuations and Noise Letters*, *4*, L195–L205.

Chacron, M. J., Longtin, A., & Maler, L. (2004c). To burst or not to burst? *Journal of Computational Neuroscience*, *17*, 127–136.

Chacron, M. J., Maler, L., & Bastian, J. (2005a). Feedback and feedforward control of frequency tuning to naturalistic stimuli. *Journal of Neuroscience*, *25*, 5521–5532.

Chacron, M. J., Maler, L., & Bastian, J. (2005b). Electroreceptor neuron dynamics shape information transmission. *Nature Neuroscience*, *8*, 673–678.

Cover, T., & Thomas, J. (1991). Elements of information theory. New York: Wiley.

Cox, D. R., & Lewis, P. A. W. (1966). The statistical analysis of series of events. London: Methuen.

Doiron, B., Laing, C., Longtin, A., & Maler, L. (2002). Ghostbursting: a novel neuronal burst mechanism. *Journal of Computational Neuroscience*, *12*, 5–25.

Doiron, B., Chacron, M. J., Maler, L., Longtin, A., & Bastian, J. (2003). Inhibitory feedback required for network oscillatory responses to communication but not prey stimuli. *Nature*, *421*, 539–543.

Fernandez, F. R., Mehaffey, W. H., & Turner, R. W. (2005). Dendritic Na+ current inactivation can increase cell excitability by delaying a somatic depolarizing afterpotential. *Journal of Neurophysiology*, *94*, 3836–3848.

Gabbiani, F., & Koch, C. (1996). Coding of time-varying signals in spike trains of integrate-and-fire neurons with random threshold. *Neural Computation*, *8*, 44–66.

Gabbiani, F., Metzner, W., Wessel, R., & Koch, C. (1996). From stimulus encoding to feature extraction in weakly electric fish. *Nature*, *384*, 564–567.

Geisler, C. D., & Goldberg, J. M. (1966). A stochastic model of the repetitive activity of neurons. *Biophysical Journal*, *6*, 53–69.

Gestri, G., Masterbroek, H. A. K., & Zaagman, W. H. (1980). Stochastic constancy, variability and adaptation of spike generation: performance of a giant neuron in the visual system of the fly. *Biological Cybernetics, 38*, 31–40.

Goldberg, J. M. (2000). Afferent diversity and the organisation of central vestibular pathways. *Experimental Brain Research, 130*, 277–297.

Hodgkin, A. L., & Huxley, A. F. (1952). A quantitative description of membrane current and its application to conduction and excitation in nerve. *Journal of Physiology London, 117*, 500–544.

Holden, A. V. (1976). *Models of the stochastic activity of neurons*. Berlin: Springer.

Jaeger, D., & Bauer, J. M. (1994). Prolonged responses in rat cerebellar Purkinje cells following activation of the granule cell layer: an intracellular *in vitro* and *in vivo* investigation. *Experimental Brain Research, 100*, 200–214.

Jolivet, R., Rauch, A., Luscher, H. R., & Gerstner, W. (2006). Predicting spike timing of neocortical pyramidal neurons by simple threshold models. *Journal of Computational Neuroscience*, *21*, 35–49.

Koch, C. (1999). *Biophysics of computation*. New York: Oxford University Press.

Köppl, C. (1997). Frequency tuning and spontaneous activity in the auditory nerve and Cochlear Nucleus Magnocellularis of the Barn Owl Tyto alba. *Journal of Neurophysiology, 77*, 364–377.

Lebedev, M. A., & Nelson, R. J. (1996). High-frequency vibratory sensitive neurons in monkey primate somatosensory cortex: entrained and nonentrained responses to vibration during the performance of vibratory-cued hand movements. *Experimental Brain Research, 111*, 313–325.

Lemon, N., & Turner, R. W. (2000). Conditional spike backpropagation generates burst discharge in a sensory neuron. *Journal of Neurophysiology, 84*, 1519–1530.

Lindner, B., Chacron, M. J., & Longtin, A. (2005). Integrate-and-fire neurons with threshold noise: A tractable model of how interspike interval correlations affect neuronal signal transmission. *Physical Review E, 72*, 021911.

Liu, Y. H., & Wang, X. J. (2001). Spike Frequency adaptation of a generalized leaky integrate-and-fire neuron. *Journal of Computational Neuroscience, 10*, 25–45.

Mainen, Z. F., & Sejnowski, T. J. (1995). Reliability of spike timing in neocortical neurons. *Science, 268*, 1503–1506.

Manwani, A., & Koch, C. (1999). Detecting and estimating signals in noisy cable structure, I: neuronal noise sources. *Neural Computation, 11*, 1797–1829.

Mar, D. J., Chow, C. C., Gerstner, W., Adams, R. W., & Collins, J. J. (1999). Noise Shaping in populations of coupled model neurons. *Proceedings of the National Academy of Sciences, 96*, 10450–10455.

Metzner, W., Koch, C., Wessel, R., & Gabbiani, F. (1998). Feature extraction by burst-like spike patterns in multiple sensory maps. *Journal of Neuroscience, 18*, 2283–2300.

Mickus, T., Jung, H. Y., & Spruston, N. (1999). Properties of slow cumulative sodium channel inactivation in rat hippocampal CA1 pyramidal neurons. *Biophysical Journal, 76*, 846–860.

Norsworthy, S. R., Schreier, R., & Temes, G. C. (Eds.) (1997). *Delta-sigma data converters*. Piscataway, NJ: IEEE Press.

Oswald, A. M. M., Chacron, M. J., Doiron, B., Bastian, J., & Maler, L. (2004). Parallel processing of sensory input by bursts and isolated spikes. *Journal of Neuroscience, 24*, 4351–4362.

Reinagel, P., & Reid, R. C. (2000). Temporal coding of visual information in the thalamus. *Journal of Neuroscience, 20*, 5392–5400.

Rieke, F., Warland, D., de Ruyter van Steveninck, R. R., & Bialek, W. (1996). *Spikes: Exploring the neural code*. Cambridge, MA: MIT.

Rudolph, M., & Destexhe, A. (2003). The discharge variability of neocortical neurons during high-conductance states. *Neuroscience, 119*, 855–873.

Sadeghi, S. G., Chacron, M. J., Taylor, M. C., & Cullen, K. E. (2007). Neural variability, detection thresholds, and information transmission in the vestibular system. *Journal of Neuroscience, 27*, 771–781.

Sah, P. (1996). Ca2+-activated K+ currents in neurones: types, physiological roles and modulation. *Trends in Neurosciences, 19*, 150–154.

Shannon, C. E. (1948). The mathematical theory of communication. *Bell Systems Technical Journal, 27*, 379–423, 623–656.

Sherman, S. M. (2001). Tonic and burst firing: dual modes of thalamocortical relay. *Trends in Neurosciences, 24*, 122–126.

Shin, J. (1993). Novel neural circuits based on stochastic pulse coding noise feedback pulse coding. *International Journal of Electronics, 74*, 359–368.

Shin, J. (2001). Adaptation in spiking neurons based on the noise shaping neural coding hypothesis. *Neural Networks, 14*, 907–919.

Shinomoto, S., Sakai, Y., & Funahashi, S. (1999). The Ornstein–Uhlenbeck process does not reproduce spiking statistics of neurons in prefrontal cortex. *Neural Computation, 11*, 935–951.

Softky, W. R., & Koch, C. (1993). The highly irregular firing of cortical cells is inconsistent with temporal integration of random EPSPs. *Journal of Neuroscience, 13*, 334–350.

Stein, R. B., Gossen, E. R., & Jones, K. E. (2005). Neuronal variability: noise or part of the signal. *Nature Reviews Neuroscience, 6*, 4766–4778.

Steriade, M. (1978). Cortical long-axoned cells and putative interneurons during the sleep-waking cycle. *Behavioural Brain Research, 3*, 465–514.

Teich, M. C. (1992). Fractal neuronal firing patterns. In: T. McKenna, J. Davis, & S. F. Zornetzer (Eds) *Single neuron computation* (pp. 589–622). San Diego: Academic Press.

Teich, M. C., & Khanna, S. M. (1985). Pulse-number distributions for the neural spike train in the cat's auditory nerve. *Journal of the Accoustical Society of America 77*, 1110–1128.

Treves, A. (1996). Mean-field analysis of neuronal spike dynamics. *Network: Computation in Neural Systems, 4*, 259–284.

Wang, X. J. (1998). Calcium coding and adaptive temporal computation in cortical pyramidal neurons. *Journal of Neurophysiology, 79*, 1549–1566.

Wiesenfeld, K., & Satija, I. (1987). Noise tolerance of frequency-locked dynamics. *Physical Review B, 36*, 2483–2492.

Yacomotti, A. M., Eguia, M. C., Aliaga, J., Martinez, O. E., & Mindlin, G. B. (1999). Interspike time distribution in noise driven excitable systems. *Physical Review Letters, 83*, 292–295.